Title: Limitations and challenges of EIT-based monitoring of stroke volume and pulmonary artery pressure.

Authors: Braun F, Proença M, Lemay M, Bertschi M, Adler A, Thiran JP, Solà J

Journal: Physiological measurement

Year: 2018 Jan 30

Issue: 39

Volume: 1

Pages: 014003

DOI: 10.1088/1361-6579/aa9828

Limitations and challenges of EIT-based monitoring of stroke volume and pulmonary artery pressure

To cite this article before publication: Fabian Braun *et al* 2017 *Physiol. Meas.* in press https://doi.org/10.1088/1361-6579/aa9828

Limitations and Challenges of EIT-Based Monitoring of Stroke Volume and Pulmonary Artery Pressure

Fabian Braun[1,2], Martin Proença[1,2], Mathieu Lemay[1], Mattia Bertschi[1], Andy Adler[3], Jean-Philippe Thiran[2,4] and Josep Solà[1]

[1] Systems Division, Swiss Center for Electronics and Microtechnology (CSEM), Neuchâtel, Switzerland

[2] Signal Processing Laboratory (LTS5), Ecole Polytechnique Fédérale de Lausanne (EPFL), Lausanne, Switzerland

[3] Systems and Computer Engineering, Carleton University, Ottawa, Canada

[4] Department of Radiology, University Hospital Center (CHUV) and University of Lausanne (UNIL), Lausanne, Switzerland

E-mail: `fbn@csem.ch`

October 2017

Abstract. *Objective*: Electrical impedance tomography (EIT) shows potential for radiation-free and noninvasive hemodynamic monitoring. However, many factors degrade the accuracy and repeatability of these measurements. Our goal is to estimate the impact of this variability on EIT-based monitoring of two important central hemodynamic parameters: stroke volume (SV) and pulmonary artery pressure (PAP).

Approach: We performed simulations on a 4D (3D + t) bioimpedance model of a human volunteer to study the influence of four potential confounding factors (electrode belt displacement, electrode detachment, changes in hematocrit and lung air volume) on the performance of EIT-based SV and PAP estimation. Results were used to estimate how these factors affect EIT measures of either absolute values or relative changes (i.e. trending).

Main results: Our findings reveal that absolute measurement of SV via EIT is very sensitive to electrode belt displacements and lung conductivity changes. Nonetheless, the trending ability of SV EIT might be a promising alternative. The timing-based measurement of PAP is more robust to lung conductivity changes but sensitive to longitudinal belt displacements at severe hypertensive levels and to rotational displacements (independent of the PAP level).

Significance: We identify and quantify challenges of EIT-based SV and PAP monitoring. These are, absolute SV via EIT is challenging but trending is feasible, while both absolute and trending of PAP via EIT are mostly impaired by belt displacements.

Keywords: electrical impedance tomography (EIT), stroke volume (SV), cardiac output

(CO), pulmonary artery pressure (PAP), bioimpedance model, simulations

1. Introduction

Since cardiovascular diseases are the major cause of death worldwide (WHO 2011), their early diagnosis and treatment is of great interest. Reliable diagnosis requires devices which allow for the accurate and harmless measurement of hemodynamic parameters to assess the health of the cardiovascular system. However, the clinical reference method for the measurement of central hemodynamic parameters – such as pulmonary artery pressure (PAP) or stroke volume (SV) – requires right heart catheterization and is known to cause complications without decreasing mortality (Harvey et al. 2005). While many alternative noninvasive approaches exist for SV monitoring, none of these have proven to be accurate enough (Joosten et al. 2017). On the other hand, the noninvasive assessment of PAP can only be performed via transthoracic echocardiography, which requires qualified personnel and is impractical for continuous measurements (Proença 2017). In view of overcoming these limitations, electrical impedance tomography (EIT) has been investigated in previous studies as a low-cost and radiation-free medical imaging modality for the noninvasive and continuous monitoring of SV (Vonk Noordegraaf et al. 2000, Pikkemaat et al. 2014) and PAP (Proença et al. 2016, Proença 2017).

Electrical impedance tomography (EIT) calculates the distribution of intra-thoracic impedance using measurements at electrodes placed on the chest surface through which small electrical currents are applied. EIT shows promise as a modality for noninvasive medical monitoring (Frerichs et al. 2017, Holder 2005). The most common thoracic application of EIT is for assessment of ventilation, as changes in alveolar air volume lead to changes in electrical impedance. EIT is also sensitive to cardiovascular activity. However, such monitoring is more challenging: First, the cardiac-related impedance changes are about one order of magnitude smaller than ventilation-related changes, and signal processing techniques must be used to separate them. Second, the exact origin of these cardiosynchronous signals remains unclear (Adler et al. 2017). Thus, for example, the EIT signal during systole has contributions from SV as well as other effects such as heart motion (Proença et al. 2015) and flow-induced reorientation of red blood cells (Gaw 2010). In this case, the EIT signal will not change in proportion to SV, if the magnitude of the other contributions are not also proportional.

EIT-based assessment of numerous hemodynamic parameters have been reported: systemic (Solà et al. 2011) and pulmonary artery pressure (Proença et al. 2016, Proença 2017), stroke volume (Vonk Noordegraaf et al. 2000, Pikkemaat et al. 2014), stroke volume variations (Maisch et al. 2011), pulmonary perfusion (Borges et al. 2012, Frerichs et al. 2009, Nguyen et al. 2012). Some studies describe limitations and challenges in cardiovascular EIT monitoring, in particular concerning the monitoring of SV. Patterson et al. (2001) concluded the cardiac EIT signal depends strongly on electrode position, lung volume and posture, in healthy volunteers. In pig experiments, Pikkemaat et al. (2014) observed variations in the subject-specific scaling of the cardiac EIT signal, which

were interpreted to stem from lung volume or heart and belt position. In a simulation study, Arshad et al. (2016) showed a strong respiration-related dependence in the EIT heart signal.

As accurate monitoring results are of importance for reliable diagnostics, our goal in this paper is to estimate the impact of these challenges on EIT-based hemodynamic monitoring. Specifically we seek to estimate the amount of uncertainty introduced into EIT-based hemodynamic parameters due to the variability in realistic clinical and ambulatory scenarios. To do so, we first list potential confounding factors and then study how seriously these factors affect the estimation of two hemodynamic parameters: stroke volume (SV), and pulmonary artery pressure (PAP). The four confounding factors selected were: (1) electrode belt displacement, (2) electrode detachment, (3) changes in hematocrit, and (4) changes in lung air volume.

In the current study we perform simulations on a 4D (3D+t) thoracic bioimpedance model – representing cardiovascular changes of a healthy human volunteer. This allows a systematic and individual investigation of potential confounding factors, which is practically impossible in real measurements. While the few limitations reported for SV monitoring via EIT are mainly based on observations from real measurements (as mentioned above), no such work is currently available at all for PAP monitoring. Thus, to the best of our knowledge, this is the first work systematically identifying and quantifying potential challenges for EIT-based SV and PAP monitoring, based on simulations on a bioimpedance model.

In section 2 we first present the bioimpedance model followed by a description of the simulations and the steps performed for signal processing and data analysis. The results are presented and discussed in section 3.

2. Methods

In the following we first describe the dynamic bioimpedance model used to perform EIT simulations. Next, we list potential confounding factors and describe the four potentially harmful ones investigated, together with other simulation parameters. Then we explain the signal processing steps used to estimate the two hemodynamic parameters (SV and PAP) from EIT image sequences. Finally, we describe the analysis applied to evaluate and quantify the decrease in performance resulting from each of the confounding factors.

2.1. Dynamic Bioimpedance Model

2.1.1. Base Model In order to simulate different hemodynamic scenarios, a dynamic bioimpedance model was created. This model is shown in Figure 1 and represents a 4D electrical conductivity distribution of a human thorax during expiratory breath-hold containing models of the heart, aorta and lungs. These models are based on magnetic resonance imaging (MRI) recordings performed on a human volunteer (62 kg, 178 cm, 28 years old). The model allows to virtually measure cardiovascular EIT with many

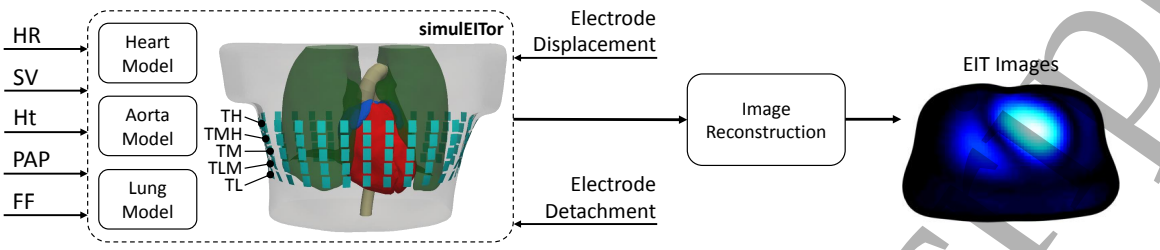

Figure 1. Block diagram of the simulation framework and the possible parameters of the bioimpedance model: heart rate (HR), stroke volume (SV), hematocrit (Ht), pulmonary artery pressure (PAP), lung filling factor (FF). The *simulEITor* framework further allows the simulation of electrode displacement and detachment.

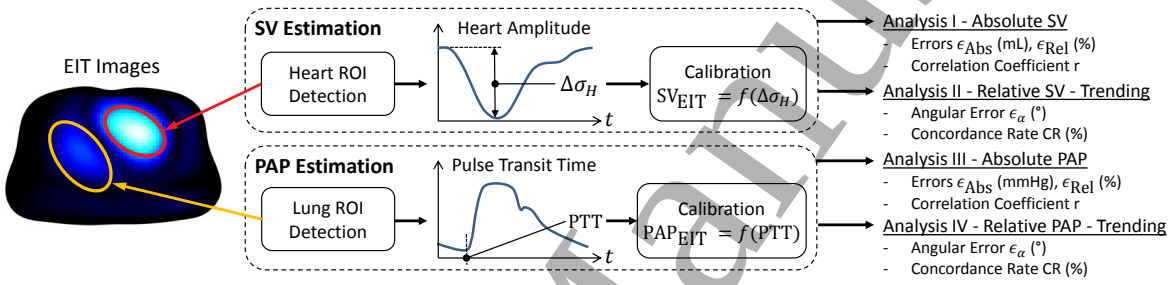

Figure 2. Block diagram of the analysis used to estimate PAP and SV from EIT image sequences.

different configurations, i.e. varying number of electrodes and their position or different voltage measurement and current injection patterns. For the present work five different EIT belts – each comprised of 32 electrodes – were applied on a transversal plane located at different levels along the craniocaudal axis as follows (see also Figure 1): (1) the TM (*transversal middle*) belt was placed at the average level of the heart, which is in between the 9-th and 10-th thoracic vertebra; The belts (2) TH (*transversal high*) and (3) TL (*transversal low*) were placed 3.5 cm higher and lower than TM, which is at the level of the 8-th (for TH) or in between the 10-th and 11-th (for TL) thoracic vertebra; The remaining two belts, (4) TMH (*transversal middle-high*) and (5) TLM (*transversal low-middle*), were placed 1.75 cm higher and lower than TM, corresponding to the 9-th (for TMH) or 10-th (for TLM) thoracic vertebra level. All simulations were performed on each belt of 32 electrodes using a bipolar stimulation pattern with four inactive electrodes between the two ones actively measuring voltage/injecting current, also known as skip 4 (Gaggero et al. 2012).

The model initially presented in (Braun et al. 2015a) was extended – as described in the following – with a more detailed heart (section 2.1.2) and pulmonary model (section 2.1.3). As in the original model (Braun et al. 2015a), skeletal muscle, fat and bones were not modeled individually but included as one intra-thoracic background conductivity composed of a mixture of 48 % muscle, 47 % fat and 5 % bone.

2.1.2. Heart Model The heart is represented by a 4D surface model of its four chambers: left/right atria/ventricles. For each of these structures a dynamic representation of its inner and outer boundaries (i.e. the endo- and epicardium) were segmented from dynamic MRI scans as described in (Braun et al. 2015b). This model was further improved in view of altering the ventricular volumes, i.e. to obtain different SVs. To this end, the volumes of the left (LV) and right ventricle (RV) were artificially modified over the entire cardiac cycle as described hereafter.

For both ventricular structures a median line was defined ranging from its apex to the center of its semilunar valve at end diastole. Then, to alternate the ventricular volume, all vertices of the corresponding model were displaced radially to the aforementioned median line. This leads to either shrinking or dilating of the corresponding ventricle. To obtain a specific ventricular volume the abovementioned procedure is applied in an iterative manner until the volume of the scaled ventricles matches the desired volume. Besides, for each iterative step, endocardial structure is scaled first and then the epicardial structure is adapted keeping a constant volume difference between the two structures and thus ensuring the quasi incompressibility of myocardial tissue (Vossoughi et al. 1980). In the present work, the SV of the left and right heart were defined to be identical: $\mathrm{SV_R} = \mathrm{EDV_R} - \mathrm{ESV_R} = \mathrm{SV_L} = \mathrm{EDV_L} - \mathrm{ESV_L}$ (with EDV and ESV as the end diastolic and end systolic volumes, respectively). Besides, a constant difference of $\mathrm{EDV_R} - \mathrm{EDV_L} = 28$ mL was set to account for the observed difference between left and right ventricular volume.

2.1.3. Pulmonary Model The spatio-temporal representation of the electrical conductivity in the lungs is based on a detailed model of the pulmonary circulation as further explained in (Proença 2017, Proença et al. 2017). This model allows the simulation of different levels of pulmonary artery pressure (PAP) and various types of pulmonary hypertensive conditions: PAH (pulmonary arterial hypertension), PHLHD (pulmonary hypertension due to left heart disease), HAPE (high altitude pulmonary edema), CTEPH (chronic thromboembolic pulmonary hypertension) (Proença 2017, Proença et al. 2017).

2.2. Simulations Performed

2.2.1. Physiological Parameters In view of mimicking physiological meaningful SV variations, different cases of changes in preload, afterload and inotropy were simulated. Initially proposed in (Proença et al. 2015, Proença 2017) and adapted to the current model, this lead to these eleven values of $\mathrm{SV_{Ref}} = [46.0, 53.4, 60.7, 60.8, 61.3, 68.0, 74.2, 74.7, 80.8, 93.5, 106.3]$ mL.

Moreover, for each of the four pulmonary pathologies supported by the current model, five levels of disease severity were simulated and compared to the normal – non-pathological – state corresponding to the following six levels of $\mathrm{PAP_{Ref}} = [14, 24, 34, 44, 54, 64]$ mmHg.

2.2.2. Investigations on Potential Confounding Factors When measuring EIT in realistic clinical or ambulatory scenarios, various factors – external (i.e. affecting the EIT system) or internal (i.e. affecting the human body under measurement) – can alter the EIT data measured and thus also the SV and PAP estimates derived thereof.

In the following we first attempt to elucidate possible factors affecting cardiovascular EIT measurements. These are: (1) electrode displacement: shifting during a measurement or misplacement between different measurements; (2) issues with electrode contact, e.g. detachment or drying out of contact gel; (3) changes in blood conductivity due to changes in hematocrit; (4) changes in lung conductivity due to respiration, liquid redistribution, extra-vascular lung water, etc.; (5) respiration-induced thorax excursion, displacement and deformation of heart, lungs and other tissues; (6) posture- and gravity-induced changes such as organ and liquid redistribution; (7) electronic noise and disturbances; (8) impedance changes due to the pulsatile reorientation of red blood cells (Gaw 2010) or other anisotropic structures, e.g. the myocardium (Adler et al. 2017).

While (5) and (7) can be – at least partly – reduced and averaged with the proper filtering technique (i.e. ECG-gated ensemble averaging), (6) might be less important when targeting bedside EIT. Due to its complexity and the assumed equally importance of the other factors, (8) was not investigated in the present work.

The remaining four potential confounding factors (1), (2), (3), and (4) were studied and are described in more detail hereafter:

(i) **Electrode belt displacement**: When using an EIT system where all electrodes are included in a belt, the whole of electrodes can be displaced in longitudinal (up/down) direction or rotated (left/right). This problem can occur during the same measurement or between different measurements where the belt needs to be reapplied – without necessarily having the knowledge of the exact belt position of the preceding measurement. For an EIT system based on gel electrodes only the latter can apply.

The TM belt (located at the height of the ventricles, see Figure 1) is considered as the "baseline" belt placement to which all the other displacements are being compared to. By using the other four belts (TL, TLM, TMH, TH) a up- and downward displacements of 1.75 and 3.5 cm were simulated.

For rotational belt displacements, two levels of magnitude were simulated by shifting the belt by 0.5 or 1.0 electrode spacing to the left/right, respectively. At the present thorax circumference of about 90 cm these shifts correspond to rotational displacements of 1.4 and 2.8 cm, respectively.

(ii) **Electrode detachment**: For various reasons (movement of the patient via internal or external influence, drying of electrode gel, *pectus excavatum*, etc.) the contact of certain EIT electrodes with the human body can be or become bad. To ensure reliable EIT images, the measurements related to these electrodes need to be removed prior to reconstruction. To this end, we simulated the detachment of each

single electrode and all possible pairs of electrodes, leading to $\binom{32}{1} + \binom{32}{2} = 528$ combinations. Failing electrodes are compensated during EIT image reconstruction with the algorithm described in (Mamatjan et al. 2013).

(iii) **Lung air volume changes**: Due to respiration, intra-thoracic conductivity distribution changes significantly between in- and expiration. To this end, we simulated four different lung air volume levels: (1) forced expiration, (2) expiration, (3) between in- and expiration, and (4) inspiration. These four levels, corresponding to filling factors of FF $= [1.3, 2.0, 3.0, 4.8]$, were simulated using lung alveolar tissue conductivities of $\sigma_{\mathrm{L}} = [0.12, 0.10, 0.08, 0.06]\ \frac{\mathrm{S}}{\mathrm{m}}$ according to (Roth et al. 2015). Even though respiratory activity normally involves other changes (i.e. deformation and/or displacement of lungs, heart and thorax) the current model simulates breath-hold and does therefore only support changes in σ_{L}.

(iv) **Hematocrit changes**: The percentage of red blood cells in the blood – known as hematocrit – does significantly influence the electrical conductivity of blood σ_{B}. To investigate the influence of hematocrit-related changes, we simulated five physiological hematocrit levels (Ht $= [35, 40, 45, 50, 55]$ %), which were transformed to the corresponding blood conductivity levels ($\sigma_{\mathrm{B}} = [0.87, 0.78, 0.70, 0.63, 0.56]\ \frac{\mathrm{S}}{\mathrm{m}}$) according to (Geddes & Sadler 1973).

2.2.3. EIT Image Reconstruction Following the pipeline illustrated in Figure 1: the raw data resulting from simulations were reconstructed into EIT images using the GREIT algorithm (Adler et al. 2009) with the recommended parameters and a noise figure of NF $= 0.5$. The reconstruction is based on a coarse version of the forward model with uniform conductivity and uses the TM belt placement.

2.3. Hemodynamic Parameter Estimation

In this section we describe the signal processing approaches to estimate SV and PAP from EIT image sequences.

2.3.1. Stroke Volume (SV) Estimation The present approach is based on hypothesis that the amplitude of the EIT heart signal is proportional to the SV, as also reported by other groups (Pikkemaat et al. 2014, Vonk Noordegraaf et al. 2000). The algorithm used is fully automatic and consists of three steps also illustrated in Figure 2: (1) determination of the heart ROI, (2) estimation of the heart sum signal amplitude $\Delta\sigma_H$ as SV surrogate measure, and (3) the calibration function.

The heart ROI is determined as follows. First, each pixel is assigned to the heart or non-heart region according to its phase at cardiac frequency (similar to the lung ROI detection in (Proença et al. 2016, Proença 2017)). Second, the potential timing of end systole is identified as the minimum of the sum signal of all potential heart pixels. Thirdly, a difference image (end diastole minus end systole) is calculated. Finally, the heart region is identified as the biggest region with positive amplitude in this difference

image where all pixels with an amplitude below an automatically determined threshold (Otsu 1979) got removed. The heart amplitude $\Delta\sigma_H$ is then computed from the sum signal in the aforementioned heart ROI as the amplitude between end diastole and end systole. The calibration transforming $\Delta\sigma_H$ from arbitrary units into $\mathrm{SV_{EIT}}$ expressed in mL is described later in section 2.4.

2.3.2. Pulmonary Artery Pressure (PAP) Estimation Our approach to measure PAP via EIT is based on the so-called pulse wave velocity principle and described in detail in (Proença et al. 2016, Proença 2017). In short, we assess the arrival of the blood pressure pulse in the distal lung region by estimating the so-called pulse transit time (PTT) – a surrogate measure for PAP having a negative exponential relationship: $\mathrm{PTT} \propto e^{-a \cdot \mathrm{PAP}}$. The algorithm used is fully automatic and consists of three steps also illustrated in Figure 2: (1) determination of the lung region of interest (ROI), (2) pixel-wise PTT estimation using Chiu's method (Chiu et al. 1991) followed by outlier removal and global PTT calculation, and (3) the calibration transforming PTT into $\mathrm{PAP_{EIT}}$ expressed in mmHg (described later in section 2.4). More details regarding this approach and the algorithm can be found in (Proença et al. 2016, Proença 2017, Proença et al. 2017).

2.4. Analysis and Performance Evaluation

To investigate the performance of the EIT-based SV and PAP estimates, we need to define figures of merit to quantitatively assess the errors caused by the aforementioned confounding factors. The influence of each of the confounding factors is assessed by comparing to the baseline configuration: TM belt, no belt displacement, no detached electrode, $\sigma_\mathrm{L} = 0.10\ \frac{\mathrm{S}}{\mathrm{m}}$ (FF = 2.0) and $\sigma_\mathrm{B} = 0.70\ \frac{\mathrm{S}}{\mathrm{m}}$ (Ht = 45 %).

2.4.1. Stroke Volume The conductivity amplitude in the heart region $\Delta\sigma_\mathrm{H}$ (computed as described in section 2.3.1), is transformed into SV values expressed in mL as follows. We first compute the linear fit ($f_H(x) = a \cdot x + b$) between the simulated SV values $\mathrm{SV_{Ref}}$ and the EIT-derived heart-amplitude $\Delta\sigma_\mathrm{H}$ of the baseline configuration. All $\Delta\sigma_\mathrm{H}$ are then transformed into SV values with exactly the same calibration function, i.e. $\mathrm{SV_{EIT}} = f_H(\Delta\sigma_\mathrm{H})$. This allows to investigate the influence of the different confounding factors while assuming an initial calibration of the EIT vs a SV reference.

In a first analysis (Analysis I), based on Bland-Altman analysis, we quantify the absolute ϵ_Abs and relative error ϵ_Rel between the estimate $\mathrm{SV_{EIT}}$ of the current vs the baseline configuration. Besides, the correlation coefficient r between $\mathrm{SV_{EIT}}$ and $\mathrm{SV_{Ref}}$ is computed. Measurements are considered as reliable if the 95 % confidence interval of ϵ_Rel does not exceed ±10 %, which is one third of the ±30 % error reported for invasive thermodilution and thus assumes averaging of at least three reference measurements as typically done in practice (Critchley 2013).

In a second analysis (Analysis II), we analyze the trending ability of the EIT-based SV values, that is the ability of $\mathrm{SV_{EIT}}$ to track changes in SV, but not absolute

values of SV. To this end, we first compute the changes of SV from an initial starting measurement and obtain the SV changes ΔSV_{EIT} and ΔSV_{Ref}, respectively. Then we plot ΔSV_{EIT} vs ΔSV_{Ref} in a 4-quadrant plot, a common methodology to asses trending ability (Critchley 2013, Saugel et al. 2015). The 4-quadrant plot was chosen over the polar plot because of its more intuitive interpretability and the fact that only noisy but not the most discordant measurements are excluded (Saugel et al. 2015). As suggested in (Saugel et al. 2015), we further quantify the trending ability by means of (1) the concordance rate CR and (2) the angular error ϵ_α. (1) CR represents the percentage of measurements where ΔSV_{EIT} and ΔSV_{Ref} change in the same direction, i.e. lie in the 1st and 3rd quadrant; (2) the angular error is defined as the angle between the identity line ($\Delta SV_{EIT} = \Delta SV_{Ref}$) and the line from the origin to the point (ΔSV_{Ref}, ΔSV_{EIT}). According to (Critchley et al. 2011) the following criteria are required to ensure acceptable trending ability: CR $> 92\,\%$, mean angular error $< \pm 5°$, confidence interval of angular error $< \pm 30°$.

2.4.2. Pulmonary Artery Pressure The pulmonary pulse transit time PTT (computed as described in section 2.3.2), is transformed into PAP values expressed in mmHg as follows. We first compute the best fit ($f_P^i(x) = a \cdot \log(x - b) + c$) between the simulated PAP_{Ref} values and the EIT-derived pulmonary PTT of the baseline configuration. A different calibration function is used for each of the four PAP pathologies simulated: $PAP_{EIT} = f_P^i(\text{PTT}), \forall\, i \in [1, 4]$. Since at higher PAP levels, small deviations of PTT can already lead to high errors in PAP, all PAP_{EIT} values above an unphysiological threshold of 100 mmHg were considered as invalid. All PTT values are then transformed into PAP values with the pathology-specific calibration function, i.e. $PAP_{EIT} = f_P^i(\text{PTT})$.

In the first PAP-related analysis (Analysis III), similar to the first SV analysis (Analysis I), we quantified the absolute ϵ_{Abs} and relative error ϵ_{Rel} by means of Bland-Altman analysis between PAP_{EIT} of the current vs the baseline configuration. Moreover, the correlation coefficient r between PAP_{EIT} and PAP_{Ref} is computed. PAP_{EIT} estimates are considered as sufficiently accurate if the 95 % confidence interval of ϵ_{Abs} falls within ± 10 mmHg (Fisher et al. 2009), which is roughly the achievable accuracy of the current noninvasive gold standard for PAP estimation, namely transthoracic echocardiography.

In the last analysis (Analysis IV), the trending ability of PAP_{EIT} was assessed. This was done analogously to Analysis II, i.e. concordance rate CR and the angular error ϵ_α were analyzed between ΔPAP_{EIT} and ΔPAP_{Ref}. The same acceptance criteria (CR $> 92\,\%$, mean angular error $< \pm 5°$, confidence interval of angular error $< \pm 30°$) as in Analysis II were applied to PAP. As these limits are designed for SV measurements (Critchley 2013), they might be too conservative, but – to the best of our knowledge – no such limits are specified for (pulmonary) blood pressure measurements.

3. Results and Discussion

3.1. Analysis I - Absolute SV

3.1.1. Belt Displacement The influence of up/down and left/right electrode belt displacement are shown in Figure 3 and the resulting errors are listed in Table 1. It can be observed that after all types of belt displacement SV_{EIT} still remains highly correlated with SV_{Ref} ($r \geq 0.99$ in Table 1, which is in line with other simulation-based studies (Dinkelbach & Stender 2015, Murphy et al. 2015).

However, the up- and downwards belt shifts introduce a significant bias in SV_{EIT}, i.e. a downwards shift leads to an increase and a upwards shift to a decrease of SV_{EIT}, respectively. This can be explained by the increase of ventricular and decrease of the pulmonary signal contribution when shifting the belt downwards, whereas the opposite applies for an upwards shift. This bias can get as high as 28.2 % and as low as −29.2 % when shifting the belt downwards or upwards by 3.5 cm, respectively.

In contrast, the errors caused by the rotational belt shifts are smaller: i.e. a leftwards shift of 2.8 cm results in a bias of 13.4 % whereas the bias for rightwards shifts is highest at 1.4 cm with only −5.3 %. The asymmetry of errors observed between left and right shifts is assumed to be due to the non-central position of the heart and the uneven distribution of lung volume between left and right.

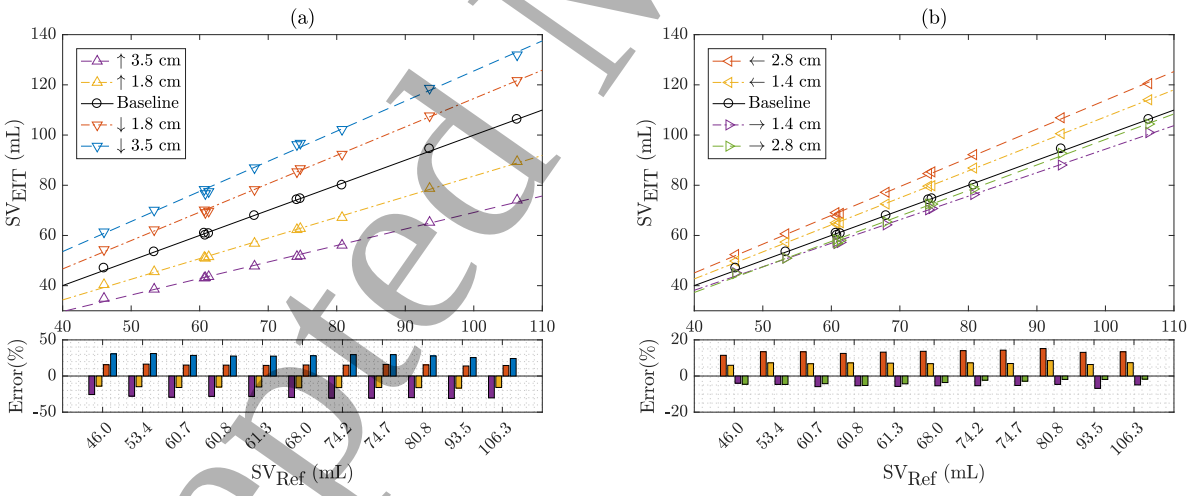

Figure 3. Influence on SV_{EIT} by (a) up/down and (b) left/right electrode belt displacements. The relationship of reference SV (SV_{Ref}) and EIT-based SV estimates (SV_{EIT}) is shown in the upper plots. The lower plots depict the relative error between SV_{EIT} and the baseline configuration.

3.1.2. Electrode Detachment The relative errors in SV_{Ref} resulting from the detachment of one or two electrodes are shown in Figure 4. The errors were calculated over the 11 SV_{Ref} simulated and are visualized per electrode to show the influence for each of the electrodes individually. Table 2 further lists the error statistics for a selection of eight electrodes when involved in the removal of two electrodes.

Table 1. Absolute error (ϵ_{Abs}), relative error (ϵ_{Rel}) and correlation coefficient (r) of SV_{EIT} for different electrode belt displacements when compared to the baseline configuration. Cell shadings indicate whether the acceptance criteria (see section 2.4.1) are met (green) or not (red).

	Up/Down Displacement				**Left/Right Displacement**			
	↑ 3.5 cm	↑ 1.8 cm	↓ 1.8 cm	↓ 3.5 cm	← 2.8 cm	← 1.4 cm	→ 1.4 cm	→ 2.8 cm
ϵ_{Abs} (mL)	-20.9 ± 6.1	-11.2 ± 3.1	10.7 ± 2.4	19.7 ± 3.7	9.6 ± 2.7	5.0 ± 1.4	-3.8 ± 1.2	-2.2 ± 0.5
ϵ_{Rel} (%)	-29.2 ± 1.6	-15.6 ± 0.8	15.2 ± 0.7	28.2 ± 2.1	13.4 ± 1.0	7.1 ± 0.7	-5.3 ± 0.8	-3.4 ± 1.3
r	0.9987	0.9993	0.9995	0.9984	0.9995	0.9998	0.9993	0.9990

The overall error is -1.08 ± 1.23 % (-0.78 ± 0.95 mL) when removing one electrode (Figure 4a) and -2.28 ± 1.79 % (-1.66 ± 1.44 mL) when removing two electrodes (Figure 4c), respectively. However, it has to be noted that detaching electrodes (1 to 4, 31 and 32) located in the ventral left region – close to the heart – results in higher errors (see also Figure 4b). These findings highlight the importance of a good electrode contact in the ventral region. In practice this can be quite challenging, especially for EIT systems having the electrodes included in a belt, where electrode contact is often impaired in the sternum region (e.g. *pectus excavatum*). This issue might be party circumvented by using more sophisticated simulation and measurement patterns or even by adapting them in real-time.

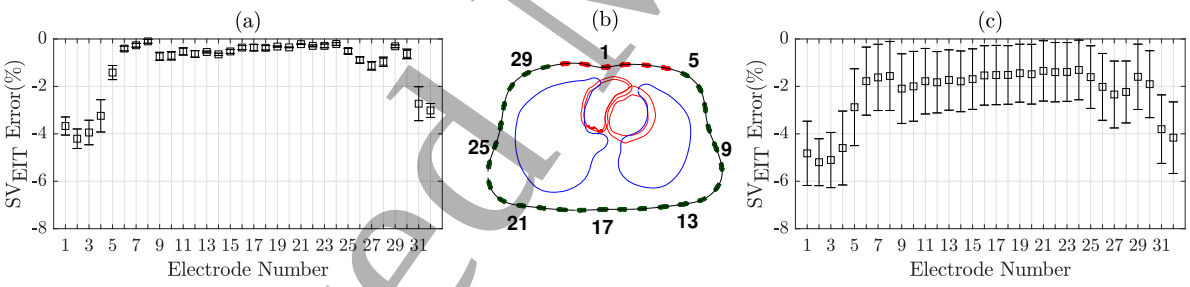

Figure 4. Relative error of SV_{EIT} resulting from the detachment of (a) a single electrode or (c) all possible pairs of electrodes. The error statistics shown are calculated over the 11 SV states simulated. The transversal EIT plane in (b) shows the position of the 32 electrodes (in green) and highlights the ones with higher errors (in red).

Table 2. Absolute error (ϵ_{Abs}), relative error (ϵ_{Rel}) and correlation coefficient (r) of SV_{EIT} resulting from the detachment of 2 electrodes when compared to the baseline configuration. Cell shadings indicate whether the acceptance criteria (see section 2.4.1) are met (green) or not (red).

	Elec. 1	**Elec. 5**	**Elec. 9**	**Elec. 13**	**Elec. 17**	**Elec. 21**	**Elec. 25**	**Elec. 29**
ϵ_{Abs} (mL)	-3.4 ± 1.4	-2.1 ± 1.4	-1.5 ± 1.2	-1.3 ± 1.0	-1.1 ± 1.0	-1.0 ± 1.0	-1.2 ± 1.1	-1.1 ± 1.1
ϵ_{Rel} (%)	-4.8 ± 1.4	-2.9 ± 1.6	-2.1 ± 1.5	-1.7 ± 1.3	-1.5 ± 1.3	-1.3 ± 1.3	-1.6 ± 1.3	-1.6 ± 1.4
r	0.9975	0.9968	0.9973	0.9978	0.9979	0.9978	0.9977	0.9976

3.1.3. Changes in Hematocrit and Lung Air Volume Figure 5a shows how changes in hematocrit influence SV_{EIT}. The corresponding errors are listed in Table 3. An increase in blood conductivity σ_B – resulting from a decrease in hematocrit – leads to a higher SV_{EIT} and in return, a decrease in σ_B to a lower SV_{EIT}. Nevertheless, the errors remain rather low, i.e. over the entire physiological range of Ht from 35 to 55 %, the relative bias changes only from 2.3 % to −3.4 %.

In contrast, changes in lung alveolar tissue conductivity σ_L – resulting from changes in lung air volume between normal inspiration and forced expiration – have a higher influence on SV_{EIT}. This is depicted in Figure 5b and also listed in Table 3. Normal inspiration ($\sigma_L = 0.06\ \frac{S}{m}$) compared to normal expiration (baseline state) introduces a relative bias of 8.0 %. On the other hand, full expiration ($\sigma_L = 0.12\ \frac{S}{m}$) lowers the bias to −3.2 %.

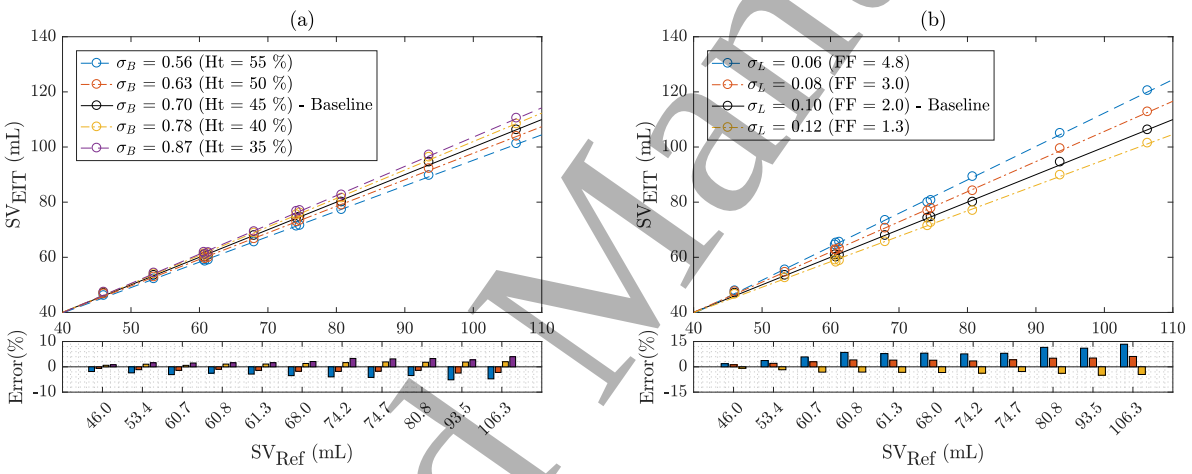

Figure 5. Influence on SV_{EIT} by changes in (a) hematocrit and (b) lung air volume. The relationship of reference SV (SV_{Ref}) and EIT-based SV estimates (SV_{EIT}) is shown in the upper plots. The lower plots depict the relative error between SV_{EIT} and the baseline configuration.

Table 3. Absolute error (ϵ_{Abs}), relative error (ϵ_{Rel}) and correlation coefficient (r) of SV_{EIT} for changes in hematocrit and lung air volume when compared to the baseline configuration. Cell shadings indicate whether the acceptance criteria (see section 2.4.1) are met (green) or not (red).

	Hematocrit Changes				**Lung Air Volume Changes**		
	$\sigma_B = 0.56$ (Ht = 55 %)	$\sigma_B = 0.63$ (Ht = 50 %)	$\sigma_B = 0.78$ (Ht = 40 %)	$\sigma_B = 0.87$ (Ht = 35 %)	$\sigma_L = 0.06$ (FF = 4.8)	$\sigma_L = 0.08$ (FF = 3.0)	$\sigma_L = 0.12$ (FF = 1.3)
ϵ_{Abs} (mL)	-2.6 ± 1.4	-1.2 ± 0.7	1.0 ± 0.6	1.8 ± 1.1	6.1 ± 3.9	2.9 ± 1.7	-2.4 ± 1.4
ϵ_{Rel} (%)	-3.4 ± 1.0	-1.5 ± 0.5	1.4 ± 0.5	2.3 ± 1.0	8.0 ± 3.3	3.9 ± 1.4	-3.2 ± 1.2
r	0.9997	0.9996	0.9995	0.9995	0.9996	0.9997	0.9993

3.1.4. Summary Among the potential confounding factors investigated for absolute SV measurement, we could show that up- and downwards electrode displacements have

the highest influence in terms of relative error, i.e. a shift of 1.8 or 3.5 cm can already introduce a relative error bias in the magnitude of about 15 or 30 %, respectively. These findings call into question the feasibility of absolute SV measurements by means of single plane (2D) EIT without recalibrating upon each displacement or reattachment of the EIT belt. The use of two EIT planes (3D) (Grychtol et al. 2016) might help to reduce the sensitivity on belt displacements in the longitudinal direction, and thus reduce the error on SV estimation in case of belt shifts. However, a subject-specific calibration is still necessary, as the absolute heart impedance signal remains influenced by various other factors (thorax morphology, lung conductivity, etc.), as also shown in experimental findings on pigs (Pikkemaat et al. 2014).

Rotational belt shifts of one electrode spacing (i.e. 2.8 cm) can introduce relative errors with a bias of up to 13 %. This highlights the importance of a correct belt placement and the necessity to have an accurate enough reconstruction model with possibly updating it (in real-time) according to the thorax morphology (Tizzard et al. 2016).

Furthermore, changes in lung alveolar tissue conductivity σ_{L} resulting simply from a respiratory cycle have shown to introduce a high bias in relative error ranging from 8 % to −3 % (from normal inspiration to full expiration). The higher the SV the higher the influence of this effect. This is because – unlike suggested by other researchers (Pikkemaat et al. 2014, Vonk Noordegraaf et al. 2000) – changes in EIT heart impedance are *not* solely related to changes in cardiac blood volume but scaled by a heart-lung-conductivity contrast and other factors (see Figure 6 for illustration and detailed explanation). Other factors such as heart displacement due to respiration or postural changes and changes of σ_{L} due to edema, pneumothorax or posture-induced liquid redistribution were not taken into account but might even worsen the current results.

These findings reveal further challenges of EIT-based SV monitoring and call for more detailed and targeted studies to assess the influences of these different confounding factors to show the extent and the conditions under which EIT-based SV is feasible in clinical scenarios at all.

The current outcomes are in line with the findings in (Eyuboglu et al. 1988). That is, absolute SV is hard, but trending should be possible. Therefore, we performed a second analysis presented in the next section assessing the trending ability of EIT-based SV.

3.2. Analysis II - Relative SV - Trending

In this section we address the question whether trending of SV via EIT is feasible, i.e. can we follow the changes in SV over time after an initial calibration with SV_0. For the subsequent analysis the baseline SV was chosen as calibration value ($\mathrm{SV}_0 = 68.0$ mL).

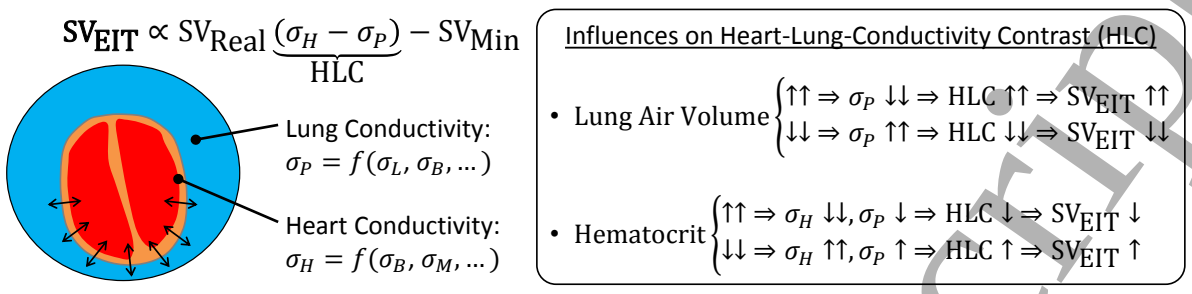

Figure 6. Conceptual explanation of the heart-lung conductivity contrast (HLC) influencing the EIT-based heart impedance signal used for estimating SV_{EIT}. During a cardiac cycle heart tissue is spatially replaced by lung tissue and vice versa (black arrows). These changes in conductivity are assumed to be the main contributor to the EIT-based heart signal. Unlike sometimes assumed this signal and thus SV_{EIT} cannot be directly proportional to the real blood volume change SV_{Real} as it is (1) scaled with the HLC and (2) limited to an inferior level of detection SV_{Min} (due to ringing and overlapping of other signal sources like the lungs or atria). HLC is defined as the difference of heart conductivity σ_H (depending on blood conductivity σ_B and myocardial conductivity σ_M) and lung conductivity σ_P (depending on lung alveolar tissue conductivity σ_L and blood conductivity σ_B). An increase in lung air volume leads to an increase in HLC and thus to an augmented SV_{EIT}, and vice versa. On the other hand, increasing hematocrit levels (Ht ↑ ⇒ σ_B ↓) lead to a decrease in σ_H and a less strong decrease of σ_P. The result is a slight decrease in HLC and a reduced SV_{EIT}. It needs to be stressed out that this remains a simplified explanation as the heart impedance signal can be influenced by further factors such as heart motion (Proença et al. 2015), out-of-(EIT-)plane motion of the heart, σ_B dependence on blood flow (Gaw 2010), anisotropy of the myocardium, etc. (Adler et al. 2017).

3.2.1. Belt Displacement The trending ability after up/down and left/right belt displacement are shown in Figure 7a and Figure 7b, respectively, by means of four quadrant plots with the corresponding errors listed in Table 4. All concordance rates CR are at 100 % and thus fulfill the first requirement for trending according to (Critchley et al. 2011). The second requirement of an angular error bias of less than 5° is only fulfilled for the 1.8 cm downwards shift and all left/right shifts. However, the angular bias resulting from a 3.5 cm downwards or 1.8 cm upwards shifts are only close above the threshold and might lead to a sufficient enough trending performance, given that the CR and the confidence interval of ϵ_α are well within the acceptable limits.

Table 4. Trending performance by means of angular error (ϵ_α) and concordance rate (CR) of SV_{EIT} as influenced by electrode belt displacements. Cell shadings indicate whether the acceptance criteria (see section 2.4.1) are met (green) or not (red).

	Up/Down Displacement				**Left/Right Displacement**			
	↓ 3.5 cm	↓ 1.8 cm	↑ 1.8 cm	↑ 3.5 cm	← 2.8 cm	← 1.4 cm	→ 1.4 cm	→ 2.8 cm
ϵ_α (°)	7.1 ± 3.0	4.3 ± 1.8	-5.7 ± 1.7	-12.5 ± 1.3	4.8 ± 1.7	2.4 ± 1.1	-1.3 ± 1.6	1.3 ± 2.1
CR (%)	100.0	100.0	100.0	100.0	100.0	100.0	100.0	100.0

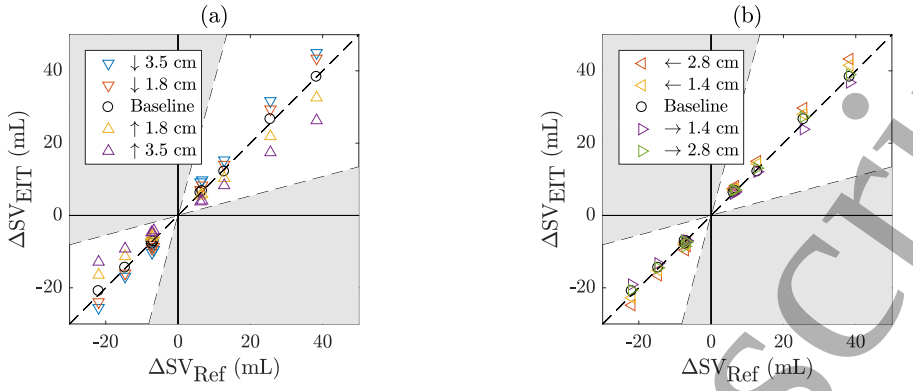

Figure 7. Trending ability of ΔSV_{EIT} vs ΔSV_{Ref} as influenced by (a) up/down and (b) left/right electrode belt displacements. The gray shaded area depicts the zone in which measurements are considered as unsuitable for trending analysis.

3.2.2. Changes in Hematocrit and Lung Air Volume The ϵ_α and CR resulting from changes in hematocrit and lung air volume are shown in Table 5 and do all fulfill the requirements for trending as specified in section 2.4.1.

Table 5. Trending performance by means of angular error (ϵ_α) and concordance rate (CR) of SV_{EIT} as influenced by hematocrit and lung air volume changes. Cell shadings indicate whether the acceptance criteria (see section 2.4.1) are met (green) or not (red).

	Hematocrit Changes				**Lung Air Volume Changes**		
	$\sigma_B = 0.56$ (Ht = 55 %)	$\sigma_B = 0.63$ (Ht = 50 %)	$\sigma_B = 0.78$ (Ht = 40 %)	$\sigma_B = 0.87$ (Ht = 35 %)	$\sigma_L = 0.06$ (FF = 4.8)	$\sigma_L = 0.08$ (FF = 3.0)	$\sigma_L = 0.12$ (FF = 1.3)
ϵ_α (°)	-2.2 ± 1.0	-0.9 ± 1.2	1.4 ± 1.4	2.4 ± 1.7	4.6 ± 1.6	2.2 ± 1.0	-1.6 ± 1.9
CR (%)	100.0	100.0	100.0	100.0	100.0	100.0	100.0

3.2.3. Summary These outcomes give hope for EIT-based trending of SV but at the same time reveal the strong influence of up/down belt displacements – especially on the angular bias. Besides, multiple confounding factors could simultaneously deteriorate SV_{EIT} (e.g. up and left belt displacement together with lung air volume changes) and thus worsen the current results. To reduce these influences we suggest the use of 3D EIT and an adaptation of the reconstruction model to the thorax geometry, as alluded to in the previous section.

3.3. Analysis III - Absolute PAP

3.3.1. Belt Displacement Figure 8 shows the influence of up/down belt displacements on PAP_{EIT} for the four pathologies simulated. The resulting errors (ϵ_{Abs} and ϵ_{Rel}) and the correlation coefficients are given in Table 6.

For most hypertensive levels – i.e. excluding the normal pressure level (PAP = 14 mmHg) – it can be observed that upwards shifts generally lead to an increase in PAP_{EIT} and downwards shifts to a decrease. This can be explained by the measurement

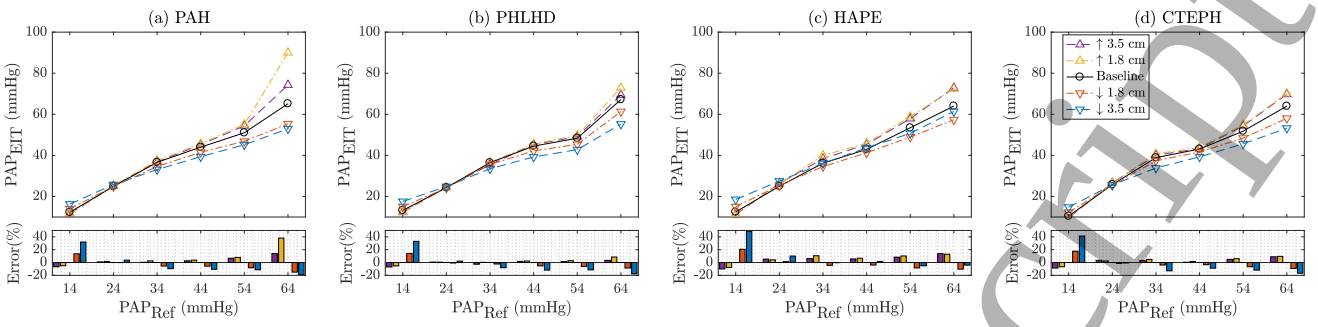

Figure 8. PAP_{EIT} estimates influenced by up/down belt displacements shown for the four pathologies simulated (a) to (d). The top row shows PAP_{EIT} in function with simulated PAP values. The bottom rows show the resulting relative error when compared to the baseline configuration.

principle used and the reduced or increased distance to the pulmonary valve – the origin of the propagating pressure pulse. On the other hand, at the normotensive level, the relative error is higher for downwards belt shifts as also shown in Table 6. We hypothesize that at higher PTT levels – as in normotension – the PTT estimation is more influenced by (ringing of) other signal sources such as the ventricular signal. This particular signal is stronger the lower the belt is placed, which would explain the increase in error for downwards shifts. The case of PAH with 1.8 cm upwards shift shows an exceptionally high error at the highest PAP level. This is due to the non-linear relationship between PTT and PAP_{EIT}, as small (negative) errors in PTT can lead to large errors in PAP_{EIT} at severely hypertensive PAP levels. If the most hypertensive level (PAP_{Ref} = 64 mmHg) is excluded from analysis (results not shown) the performances of all upwards and 1.8 cm downwards shifts fall within the acceptance criteria and only the 3.5 cm downwards shifts remain out of the acceptable limits.

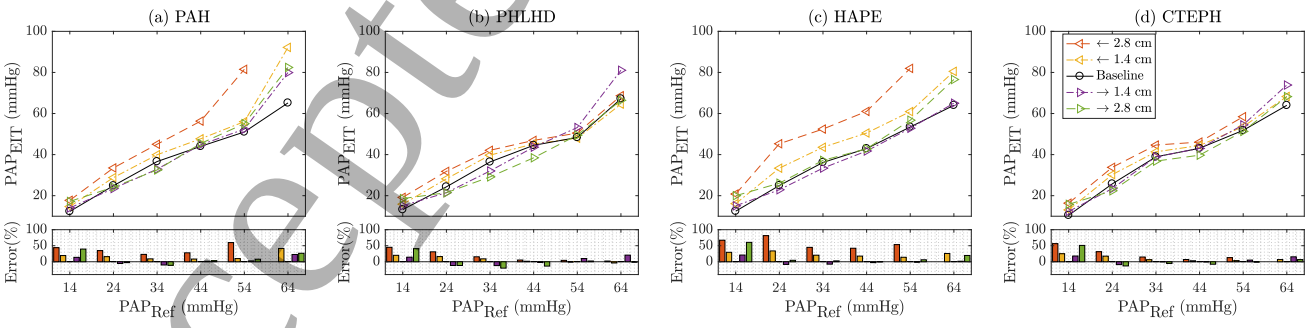

Figure 9. PAP_{EIT} estimates influenced by left/right belt displacements shown for the four pathologies simulated (a) to (d). The top row shows PAP_{EIT} in function with simulated PAP values. The bottom rows show the resulting relative error when compared to the baseline configuration.

The errors resulting from left/right belt shifts are given in Figure 9 and also listed in Table 6. In contrast to up/down belt shifts, the left/right shifts generally result in higher errors of PAP_{EIT}. The magnitude of error caused by slight rotational shifts (1.4 or 2.8

cm, i.e. 0.5 or 1.0 electrode spacing) are surprising and the reason not fully understood but clearly linked to the reconstruction model used. A possible explanation is that small discrepancies of thorax geometries (between the real thorax geometry and the reconstruction model geometry) result in spatial mixing of the different signal sources, i.e. a higher contribution of ventricular or atrial signals in the lung region. This in turn deteriorates the pulmonary signal and estimation of the correct PTT is impaired.

With exception of (b) PHLHD, the other pathologies lead to unphysiological high PAP_{EIT} values at the highest PAP_{Ref} level which were excluded from analysis (marked with a (†) in Table 6). They thus show a higher error in PAP_{EIT} for leftwards belt shifts when compared to rightwards shifts, which is consistent with the findings for SV_{EIT} presented in the previous sections. Again, if the most hypertensive level ($PAP_{Ref} = 64\,mmHg$) is excluded from analysis (results not shown) the performances improves such that from previously 6, already 12 out of 16 errors fall within the acceptance criteria defined in section 2.4.2.

Table 6. Absolute error (ϵ_{Abs}), relative error (ϵ_{Rel}) and correlation coefficient (r) of PAP_{EIT} for different electrode belt displacements when compared to the baseline configuration. This is shown for each of the four pathologies: (a) PAH, (b) PHLHD, (c) HAPE, and (d) CTEPH. Cells marked with (†) indicate that one PAP_{EIT} value was above the unphysiological threshold of 100 mmHg (see section 2.4.2) and excluded from analysis. Cell shadings indicate whether the acceptance criteria (see section 2.4.2) are met (green) or not (red).

		Up/Down Displacement				**Left/Right Displacement**			
		↑ 3.5 cm	↑ 1.8 cm	↓ 1.8 cm	↓ 3.5 cm	← 2.8 cm	← 1.4 cm	→ 1.4 cm	→ 2.8 cm
(a)	ϵ_{Abs} (mmHg)	2.2 ± 3.7	5.2 ± 9.8	-2.8 ± 4.0	-3.6 ± 5.6	13.1 ± 10.1 (†)	7.6 ± 9.6	2.3 ± 6.5	3.8 ± 7.4
	ϵ_{Rel} (%)	3.1 ± 6.9	8.1 ± 15.3	-3.5 ± 9.7	-2.4 ± 18.4	37.9 ± 14.6 (†)	17.3 ± 12.6	4.2 ± 12.2	10.5 ± 19.0
	r	0.9916	0.9639	0.9933	0.9969	0.9871 (†)	0.9570	0.9741	0.9690
(b)	ϵ_{Abs} (mmHg)	0.3 ± 1.2	1.3 ± 2.3	-1.7 ± 2.6	-3.5 ± 5.6	4.2 ± 2.5	1.3 ± 2.5	2.1 ± 6.7	-1.7 ± 4.7
	ϵ_{Rel} (%)	-0.4 ± 3.8	1.6 ± 4.5	-1.5 ± 8.2	-2.3 ± 18.5	17.3 ± 17.3	7.0 ± 9.6	3.2 ± 13.8	-0.6 ± 21.8
	r	0.9864	0.9818	0.9860	0.9902	0.9766	0.9794	0.9701	0.9739
(c)	ϵ_{Abs} (mmHg)	3.0 ± 3.4	3.4 ± 3.3	-1.9 ± 3.3	0.6 ± 3.3	18.3 ± 7.3 (†)	8.5 ± 4.3	-0.5 ± 2.0	4.2 ± 4.9
	ϵ_{Rel} (%)	4.9 ± 8.0	6.2 ± 7.5	-0.8 ± 11.3	8.5 ± 20.5	57.8 ± 16.4 (†)	23.5 ± 7.5	0.4 ± 10.7	15.6 ± 23.1
	r	0.9953	0.9951	0.9978	0.9986	0.9770 (†)	0.9880	0.9975	0.9775
(d)	ϵ_{Abs} (mmHg)	1.6 ± 2.3	2.0 ± 2.4	-1.8 ± 2.7	-3.6 ± 5.2	5.9 ± 1.8 (†)	2.8 ± 1.3	2.0 ± 4.2	0.0 ± 3.8
	ϵ_{Rel} (%)	2.0 ± 5.9	3.0 ± 5.5	-1.1 ± 9.6	-1.6 ± 21.7	24.5 ± 20.0 (†)	10.4 ± 8.9	4.9 ± 10.2	5.1 ± 23.4
	r	0.9859	0.9861	0.9864	0.9938	0.9664 (†)	0.9819	0.9877	0.9842

3.3.2. Electrode Detachment The error in PAP_{EIT} resulting from removing single or pairs of electrodes is shown in Figure 10 by the example of the PHLHD pathology. Table 7 further lists the error statistics for a selection of eight electrodes when involved in the removal of two electrodes. Detaching one single electrode leads to an error of 1.73 ± 3.76 % (1.10 ± 2.26 mmHg) (Figure 10a) and detaching pairs of electrodes to an error of 2.08 ± 4.49 % (1.25 ± 2.65 mmHg) (Figure 10c). The error remains low for all

electrodes with slightly higher errors for some electrodes located ventrally and on the right as shown in Figure 10b.

The absolute and relative errors of the other three pathologies are lower (results not shown) than for the PHLHD pathology shown here.

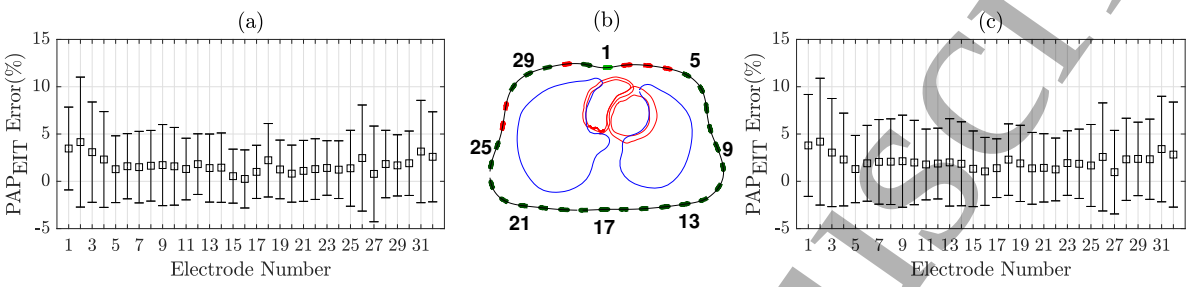

Figure 10. Relative error of PAP_{EIT} resulting from the detachment of (a) a single electrode or (c) all possible pairs of electrodes. The error statistics shown are calculated over the 6 PAP states simulated for the PHLHD pathology. The transversal EIT plane in (b) shows the position of the 32 electrodes (in green) and highlights the six electrodes with highest errors (in red).

Table 7. Absolute error (ϵ_{Abs}), relative error (ϵ_{Rel}) and correlation coefficient (r) of PAP_{EIT} resulting from the detachment of 2 electrodes when compared to the baseline configuration (PHLHD pathology). Cell shadings indicate whether the acceptance criteria (see section 2.4.2) are met (green) or not (red).

Name	**Elec. 1**	**Elec. 5**	**Elec. 9**	**Elec. 13**	**Elec. 17**	**Elec. 21**	**Elec. 25**	**Elec. 29**
ϵ_{Abs} (mmHg)	1.6 ± 2.6	0.9 ± 2.0	1.4 ± 3.0	1.3 ± 2.8	0.9 ± 1.8	0.9 ± 2.1	1.2 ± 2.6	1.1 ± 2.1
ϵ_{Rel} (%)	3.8 ± 5.4	1.3 ± 3.6	2.1 ± 4.9	2.0 ± 4.6	1.4 ± 3.1	1.4 ± 3.6	1.7 ± 4.3	2.4 ± 3.9
r	0.9754	0.9774	0.9731	0.9733	0.9781	0.9765	0.9746	0.9771

3.3.3. Changes in Hematocrit and Lung Air Volume Figure 11 shows PAP_{EIT} as influenced by changes in hematocrit and lung air volume by the example of the PHLHD pathology. The resulting relative errors are also listed in Table 8. While the error induced by hematocrit changes remains low, lung air volume changes can induce errors up to -6.7 ± 3.7 %. This could again be explained by the aforementioned influence of other signal sources deteriorating the PTT estimation. As shown for SV in section 3.1.3, the amplitude of the heart signal is more affected by changes in air volume than by changes in hematocrit, which would explain the higher errors in PAP_{EIT} for the former when compare to the latter. Nevertheless, all errors fulfill the acceptance criteria defined in section 2.4.2.

3.3.4. Summary We could show that for belt displacements PAP_{EIT} is highly sensitive to small errors of PTT at severe hypertensive levels which translate into high errors in PAP_{EIT} due to the negative exponential relationship between PTT and PAP_{EIT}. Yet, when not considering the most hypertensive level at 64 mmHg, PAP_{EIT} is robust to

Table 8. Absolute error (ϵ_{Abs}), relative error (ϵ_{Rel}) and correlation coefficient (r) of PAP_{EIT} for the PHLHD pathology as influenced by changes in hematocrit and lung air volume when compared to the baseline configuration. Cell shadings indicate whether the acceptance criteria (see section 2.4.2) are met (green) or not (red).

	Hematocrit Changes				**Lung Air Volume Changes**		
	$\sigma_B = 0.56$ (Ht = 55 %)	$\sigma_B = 0.63$ (Ht = 50 %)	$\sigma_B = 0.78$ (Ht = 40 %)	$\sigma_B = 0.87$ (Ht = 35 %)	$\sigma_L = 0.06$ (FF = 4.8)	$\sigma_L = 0.08$ (FF = 3.0)	$\sigma_L = 0.12$ (FF = 1.3)
ϵ_{Abs} (mmHg)	-0.0 ± 0.5	-0.2 ± 0.3	0.0 ± 0.1	0.1 ± 0.2	-3.1 ± 2.2	-1.6 ± 1.2	1.7 ± 1.6
ϵ_{Rel} (%)	-0.1 ± 1.1	-0.5 ± 0.7	0.1 ± 0.4	0.2 ± 0.6	-6.7 ± 3.7	-3.3 ± 2.1	3.5 ± 2.2
r	0.9858	0.9881	0.9867	0.9859	0.9898	0.9892	0.9816

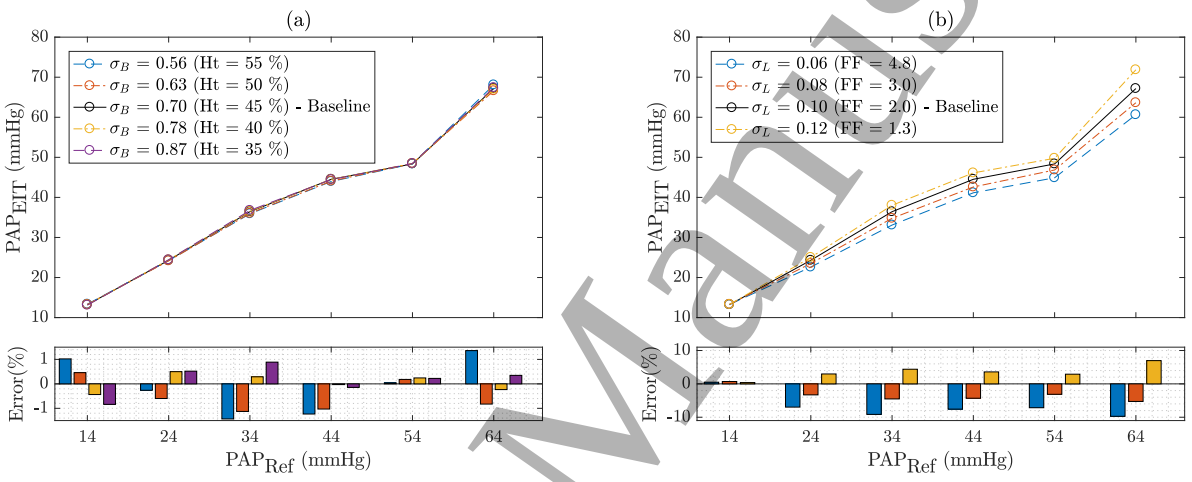

Figure 11. PAP_{EIT} estimates for PHLHD pathology as influenced by (a) hematocrit, (b) lung air volume. The top row shows PAP_{EIT} in function with simulated PAP values. The bottom rows show the resulting relative error when compared to the baseline configuration.

most up/down belt displacements with the exception of downwards shifts of 3.5 cm for which the pulmonary signal gets too low and other signal sources prevail. However, the errors resulting from rotational belt shifts remain surprisingly high and their cause is not yet fully understood but is assumed to be linked to the mismatch between real thorax geometry and the one of the reconstruction model. We hypothesize that already small rotations (0.5 or 1.0 electrode spacing) increase the spatial overlap/mixing of different signal sources contributing cardiovascular EIT. This issue requires further investigations which falls out of scope of the current work.

In general, measuring PAP_{EIT} via PTT – a timing-based feature – is more robust to changes in lung conductivity than the amplitude-based SV_{EIT} estimation. However, it is sensitive to longitudinal belt displacements at severe hypertensive levels and to rotational displacements (independent of the PAP level).

3.4. Analysis IV - Relative PAP - Trending

Analogous to the SV trending analysis (Analysis II in section 3.2) we assess whether trending of PAP_{EIT} is feasible, i.e. can we follow the changes in PAP over time after an initial calibration with PAP_0. For the subsequent analysis the normotensive PAP level was chosen as calibration value ($PAP_0 = 14\,mmHg$).

3.4.1. Belt Displacement The trending ability after up/down and left/right belt displacement are shown in Figure 12 by means of four quadrant plots with the corresponding errors listed in Table 9. While all concordance rates CR are at 100 % and the confidence interval of ϵ_α within the $< \pm 30°$ limits, the acceptable threshold of $< \pm 5°$ for the angular bias is often exceeded.

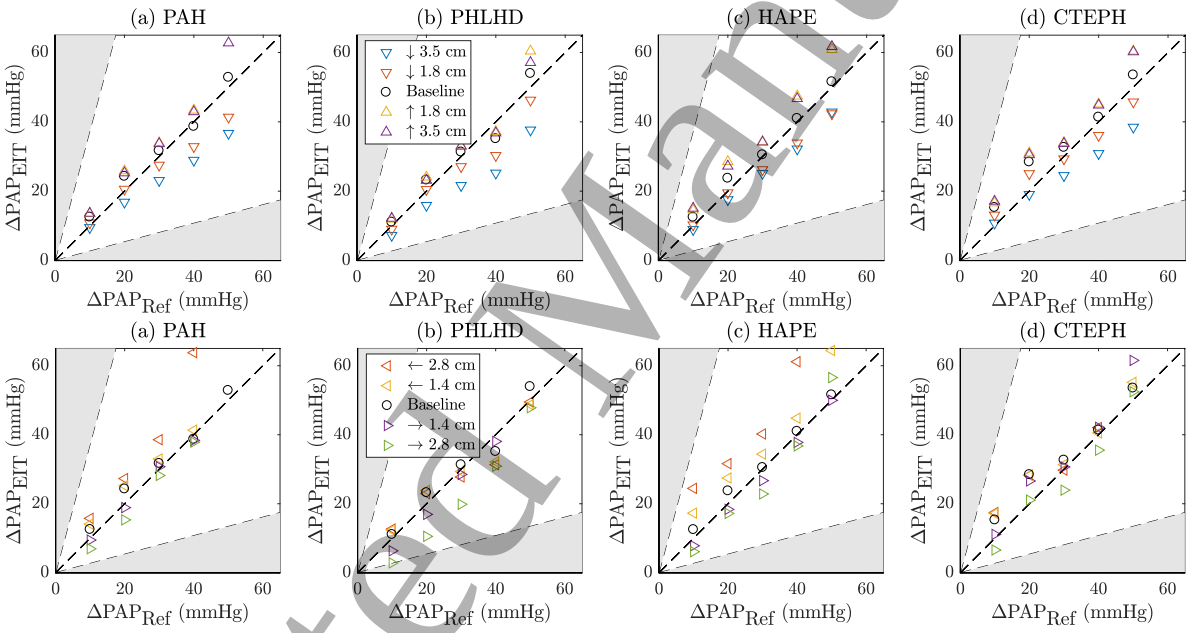

Figure 12. Trending ability of PAP_{EIT} vs PAP_{Ref} as influenced by (Top) up/down and (Bottom) left/right electrode belt displacements shown for the four pathologies simulated (a) to (d). The gray shaded area depicts the zone in which measurements are considered as unsuitable for trending analysis.

3.4.2. Changes in Hematocrit and Lung Air Volume The ϵ_α and CR resulting from changes in hematocrit and lung air volume are shown in Table 10 by the example of the PHLHD pathology. They do all fulfill the requirements specified for trending of PAP_{EIT}.

3.4.3. Summary Considering belt displacements, the high errors observed for absolute PAP monitoring (mostly for leftwards shifts), also impair the trending ability of PAP_{EIT} by introducing a high angular bias and require further investigations. Many of the other belt displacements also result in an angular bias slightly exceeding the $< \pm 5°$ limit and thus – strictly speaking – do not fulfill the requirements for trending. However, it

Table 9. Trending performance by means of angular error (ϵ_α) and concordance rate (CR) of PAP_{EIT} as influenced by electrode belt displacements. This is shown for each of the four pathologies: (a) PAH, (b) PHLHD, (c) HAPE, and (d) CTEPH. Cells marked with (†) indicate that one PAP_{EIT} value was above the unphysiological threshold of 100 mmHg (see section 2.4.2) and excluded from analysis. Cell shadings indicate whether the acceptance criteria (see section 2.4.2) are met (green) or not (red).

		Up/Down Displacement				**Left/Right Displacement**			
		$\downarrow$ 3.5 cm	$\downarrow$ 1.8 cm	$\uparrow$ 1.8 cm	$\uparrow$ 3.5 cm	$\leftarrow$ 2.8 cm	$\leftarrow$ 1.4 cm	$\rightarrow$ 1.4 cm	$\rightarrow$ 2.8 cm
(a)	ϵ_α (°)	-6.3 ± 3.2	-2.1 ± 3.6	6.8 ± 4.1	5.4 ± 2.7	10.4 ± 2.9 (†)	6.4 ± 4.7	0.8 ± 4.0	-2.7 ± 6.8
	CR (%)	100.0	100.0	100.0	100.0	100.0 (†)	100.0	100.0	100.0
(b)	ϵ_α (°)	-9.1 ± 2.3	-3.0 ± 3.1	3.3 ± 3.2	2.8 ± 3.1	0.2 ± 5.3	0.7 ± 5.0	-2.5 ± 7.3	-13.3 ± 10.6
	CR (%)	100.0	100.0	100.0	100.0	100.0	100.0	100.0	100.0
(c)	ϵ_α (°)	-4.5 ± 1.2	-2.6 ± 2.5	6.9 ± 3.0	6.8 ± 3.2	13.9 ± 6.2 (†)	7.6 ± 4.7	-2.9 ± 2.6	-4.9 ± 6.3
	CR (%)	100.0	100.0	100.0	100.0	100.0 (†)	100.0	100.0	100.0
(d)	ϵ_α (°)	-3.9 ± 4.2	1.6 ± 5.1	7.7 ± 5.0	7.7 ± 5.2	6.5 ± 7.2 (†)	5.8 ± 6.2	3.8 ± 3.1	-3.7 ± 5.5
	CR (%)	100.0	100.0	100.0	100.0	100.0 (†)	100.0	100.0	100.0

Table 10. Trending performance – for the PHLHD pathology – by means of angular error (ϵ_α) and concordance rate (CR) of PAP_{EIT} as influenced by hematocrit and lung air volume changes. Cell shadings indicate whether the acceptance criteria (see section 2.4.2) are met (green) or not (red).

	Hematocrit Changes				**Lung Air Volume Changes**		
	$\sigma_B = 0.56$ (Ht = 55 %)	$\sigma_B = 0.63$ (Ht = 50 %)	$\sigma_B = 0.78$ (Ht = 40 %)	$\sigma_B = 0.87$ (Ht = 35 %)	$\sigma_L = 0.06$ (FF = 4.8)	$\sigma_L = 0.08$ (FF = 3.0)	$\sigma_L = 0.12$ (FF = 1.3)
ϵ_α (°)	1.0 ± 2.9	1.0 ± 2.8	1.5 ± 3.1	1.7 ± 3.2	-2.5 ± 2.4	-0.6 ± 2.7	3.0 ± 3.4
CR (%)	100.0	100.0	100.0	100.0	100.0	100.0	100.0

is questionable whether the acceptance criteria specified – originally proposed for SV monitoring (Critchley et al. 2011) – are not too strict for the application of noninvasive PAP monitoring. Depending on the use case, a higher angular bias could be acceptable, especially when taking into account the other advantages of EIT-based PAP monitoring (operator independent, fully automatic, continuous application) when compared to the current noninvasive gold standard (transthoracic echocardiography).

3.5. Limitations and Future Work

The present work is limited in that the hemodynamic bioimpedance model used could only be partially validated. That is, the findings from simulations on the initial model regarding EIT-derived PAP estimation (Proença et al. 2017) have been confirmed by practical measurements (Proença et al. 2016). However – although directly derived from real MRI scans – the heart model allowing for SV changes was not validated against real EIT measurements. Therefore, we suggest to confirm the current findings by validating against real EIT measurements for future work.

The bioimpedance model is further limited in that it is solely based on the end expiratory breath-hold state and no respiration-related displacements and deformations

can be simulated. More detailed insights might be obtained from a more extensive model (e.g. (Segars et al. 2010) used in (Murphy et al. 2015)) incorporating thoracic excursions, lung deformation, heart deformation and displacement (i.e. out of plane motion (Zhang et al. 2013)) – all modulated by respiration. Moreover, the present SV modifications were generated artificially. A statistically more representative model covering variations of multiple individuals might be of advantage. Besides, while skeletal muscles, fat, bones and skin were only considered in the homogeneous background conductivity (excluding the skin), these should be modeled as individual structures in the future.

In addition, posture-induced heart displacement and lung liquid distribution, such as pneumothorax or edema should be studied as they could be additional confounding factors for EIT based SV monitoring. Even though we have only investigated a part of all possible confounding factors, we believe to have revealed some important challenges for SV via EIT mostly due to belt displacements and the heart-lung-conductivity contrast. Future clinical studies aiming for SV_{EIT} should concentrate on the use of 3D EIT, constant ventilator settings and posture to avoid most of the confounding factors observed here from occurring, and then – in a next step – investigate the influence of each of the factors individually.

In contrary to the amplitude-based feature SV_{EIT}, PAP_{EIT} is measured via PTT – a timing-based feature (Solà & Brunner 2012, Solà et al. 2012). It is therefore not surprising that EIT-based PAP estimation by means of pulmonary PTT has shown to be less influenced by changes in hematocrit or lung air volume. Nonetheless, the strong deteriorating influence resulting from rotational belt displacements require further investigations and special attention. Moreover, the acceptance criteria specified for PAP trending, are initially designed for SV trending and might be too restrictive, in particular the threshold for the angular bias.

4. Conclusion

In this paper, we focus on the problem of uncertainty introduced into EIT-based hemodynamic measures due to variability in configuration and physiology which occur in experimental and clinical use. Our goal was to estimate the level of uncertainty in two important central hemodynamic parameters due to the most important confounding factors. To this end, we investigated EIT-based hemodynamic monitoring of SV and PAP, for the four confounding factors potentially deteriorating these measures: (1) electrode belt displacement, (2) electrode detachment, changes in (3) hematocrit and (4) lung air volume. Based on simulations on a 4D bioimpedance model, we could show how seriously each of these factors affect the estimation of relative or absolute PAP and SV, as also summarized in Table 11.

The amplitude-based feature to assess SV is highly sensitive to – mostly up/down – belt displacements and to variations in lung air volume. Although these limitations might be partly overcome by using 3D EIT, our results indicate that the absolute measurement of SV via EIT remains extremely challenging. Nonetheless, we can

conclude that the trending ability of SV_{EIT} – that is following changes in SV after an initial calibration – remains promising.

On the contrary, the timing-based measurement of PAP is more robust to lung conductivity changes but sensitive to longitudinal belt displacements at severe hypertensive levels and to rotational displacements (independent of the PAP level). The latter requires particular attention in further investigations.

The present work is limited in that the hemodynamic bioimpedance model was not fully validated. Therefore, the current findings remain to be confirmed by means of real EIT measurements in future work.

Table 11. Findings of the SV and PAP analyses performed for the four confounding factors investigated. The results are classified according to the percentage falling within the acceptance criteria: ✓ 100 % (good); ✗ ≥ 75 % (mediocre); ✗✗ < 75 % (bad).

	SV		PAP	
	Absolute *Analysis I*	Relative *Analysis II*	Absolute *Analysis III*	Relative *Analysis IV*
1. Belt displacement up/down	✗✗	✗✗	✗✗	✗✗
1. Belt displacement left/right	✗	✓	✗✗	✗✗
2. Electrode detachment	✓		✓	
3. Hematocrit changes	✓	✓	✓	✓
4. Lung air volume changes	✗✗	✓	✓	✓

Acknowledgments

This work was made possible by grants from the SNSF/Nano-Tera project OBESENSE (20NA21-1430801) and the Swiss National Science Foundation (SNSF, no. 205321_153364/1). We would like to thank Yasin Mamatjan and Beat Müller for their help with the implementation of the failing electrode detachment algorithm. Moreover, we would like to show our gratitude to Xenia Alba, Karim Lekadir and Alejandro F. Frangi for performing the MRI segmentation of the 4D heart model.

References

Adler A, Arnold J H, Bayford R, Borsic A, Brown B, Dixon P, Faes T J C, Frerichs I, Gagnon H, Gärber Y, Grychtol B, Hahn G, Lionheart W R B, Malik A, Patterson R P, Stocks J, Tizzard A, Weiler N & Wolf G K 2009 *Physiological Measurement* **30**(6), S35–S55.

Adler A, Proença M, Braun F, Brunner J & Solà J 2017 *in* 'Proceedings of the 18th International Conference on Biomedical Applications of Electrical Impedance Tomography' Zenodo Dartmouth, Hanover, New Hampshire, USA, p. 73.

Arshad S H, Murphy E K & Halter R J 2016 *in* 'Proc. SPIE 9788, Medical Imaging 2016', p. 97882D.

Borges J B, Suarez-Sipmann F, Bohm S H, Tusman G, Melo A, Maripuu E, Sandstrom M, Park M, Costa E L V, Hedenstierna G & Amato M 2012 *Journal of Applied Physiology* **112**(1), 225–236.

Braun F, Proença M, Rapin M, Alba X, Lekadir K, Lemay M, Solà J, Frangi A F & Thiran J P 2015b *in* 'Proceedings of the 16th International Conference on Biomedical Applications of Electrical Impedance Tomography' Zenodo Neuchâtel, Switzerland, p. 107.

Braun F, Proença M, Rapin M, Lemay M, Adler A, Grychtol B, Solà J & Thiran J P 2015a *Physiological Measurement* **36**(6), 1147–1159.

Chiu Y, Arand P W, Shroff S G, Feldman T & Carroll J D 1991 *American Heart Journal* **121**(5), 1460–1470.

Critchley L A 2013 *in* W. S Aronow, ed., 'Artery Bypass' InTech. DOI: 10.5772/54413.

Critchley L A, Yang X X & Lee A 2011 *Journal of Cardiothoracic and Vascular Anesthesia* **25**(3), 536–546.

Dinkelbach J & Stender B 2015 *in* 'Proceedings of the 16th International Conference on Biomedical Applications of Electrical Impedance Tomography' Zenodo Neuchâtel, Switzerland, p. 109.

Eyuboglu B M, Brown B H & Barber D C 1988 *Clinical Physics and Physiological Measurement* **9**(4A), 71.

Fisher M R, Forfia P R, Chamera E, Housten-Harris T, Champion H C, Girgis R E, Corretti M C & Hassoun P M 2009 *American Journal of Respiratory and Critical Care Medicine* **179**(7), 615–621.

Frerichs I, Amato M B P, van Kaam A H, Tingay D G, Zhao Z, Grychtol B, Bodenstein M, Gagnon H, Böhm S H, Teschner E, Stenqvist O, Mauri T, Torsani V, Camporota L, Schibler A, Wolf G K, Gommers D, Leonhardt S, Adler A & TREND study group 2017 *Thorax* **72**(1), 83–93.

Frerichs I, Pulletz S, Elke G, Reifferscheid F, Schädler D, Scholz J & Weiler N 2009 *Respiration* **77**(3), 282–291.

Gaggero P O, Adler A, Brunner J & Seitz P 2012 *Physiological Measurement* **33**(5), 831–847.

Gaw R L 2010 The effect of red blood cell orientation on the electrical impedance of pulsatile blood with implications for impedance cardiography PhD thesis Queensland University of Technology. https://eprints.qut.edu.au/39448/.

Geddes L A & Sadler C 1973 *Medical and Biological Engineering and Computing* **11**(3), 336–339.

Grychtol B, Müller B & Adler A 2016 *Physiological Measurement* **37**(6), 785–800.

Harvey S, Harrison D A, Singer M, Ashcroft J, Jones C M, Elbourne D, Brampton W, Williams D, Young D & Rowan K 2005 *The Lancet* **366**(9484), 472–477.

Holder D, ed. 2005 *Electrical impedance tomography: methods, history, and applications* Series in medical physics and biomedical engineering Institute of Physics Pub Bristol, UK. DOI: 10.1201/9781420034462.

Joosten A, Desebbe O, Suehiro K, Murphy L S L, Essiet M, Alexander B, Fischer M O, Barvais L, Van Obbergh L, Maucort-Boulch D & Cannesson M 2017 *BJA: British Journal of Anaesthesia* **118**(3), 298–310.

Maisch S, Bohm S H, Solà J, Goepfert M S, Kubitz J C, Richter H P, Ridder J, Goetz A E & Reuter D A 2011 *Critical Care Medicine* **39**(9), 2173–2176.

Mamatjan Y, Gaggero P, Grychtol B & Adler A 2013 *in* 'CMBES conference' Ottawa, Canada.

Murphy E, Halter R & Odame K 2015 *in* 'Biomedical Engineering Conference (NEBEC), 2015 41st Annual Northeast' IEEE, pp. 1–2.

Nguyen D T, Jin C, Thiagalingam A & McEwan A L 2012 *Physiological Measurement* **33**(5), 695–706.

Otsu N 1979 *IEEE Transactions on Systems, Man, and Cybernetics* **9**(1), 62–66.

Patterson R P, Zhang J, Mason L I & Jerosch-Herold M 2001 *Physiological Measurement* **22**(1), 159.

Pikkemaat R, Lundin S, Stenqvist O, Hilgers R D & Leonhardt S 2014 *Anesthesia & Analgesia* **119**(1), 76–83.

Proença M 2017 Non-invasive hemodynamic monitoring by electrical impedance tomography PhD thesis École Polytechnique Fédérale de Lausanne. DOI: 10.5075/epfl-thesis-7444.

Proença M, Braun F, Rapin M, Solà J, Adler A, Grychtol B, Bohm S H, Lemay M & Thiran J P 2015 *Physiological Measurement* **36**(6), 1075–1091.

Proença M, Braun F, Solà J, Adler A, Lemay M, Thiran J P & Rimoldi S F 2016 *Physiological*

Measurement **37**(6), 713–726.

Proença M, Braun F, Solà J, Thiran J P & Lemay M 2017 *Medical & Biological Engineering & Computing* **55**(6), 949–963.

Roth C J, Ehrl A, Becher T, Frerichs I, Schittny J C, Weiler N & Wall W A 2015 *Physiological Measurement* **36**(6), 1211–1226.

Saugel B, Grothe O & Wagner J Y 2015 *Anesthesia & Analgesia* **121**(2), 514–524.

Segars W P, Sturgeon G, Mendonca S, Grimes J & Tsui B M W 2010 *Medical Physics* **37**(9), 4902–4915.

Solà J, Adler A, Santos A, Tusman G, Sipmann F S & Bohm S H 2011 *Medical & Biological Engineering & Computing* **49**(4), 409–415.

Solà J & Brunner J 2012 'Method and Apparatus for Time-Based Analysis of Electrical Impedance Tomography Data'. Patent, WO/2012/007425.

Solà J, Brunner J, Ferrario D & Adler A 2012 'Method and Apparatus for the Non-Invasive Measurement of Pulse Transit Times (PTT)'. Patent, WO/2012/007423.

Tizzard A, Demosthenous A & Bayford R 2016 *in* '16th International Conference on Electrical Bio-Impedance (ICEBI)' Stockholm, Sweden, p. 128.

Vonk Noordegraaf A, Janse A, Marcus J T, Bronzwaer J G, Postmus P E, Faes T J & de Vries P M 2000 *Physiological measurement* **21**(2), 285.

Vossoughi J, Vaishnav R N & Patel D J 1980 *Adv Bioeng* **1980**, 45–48.

WHO 2011 *A prioritized research agenda for prevention and control of noncommunicable diseases.* World Health Organization Geneva. ISBN: 978-92-4-156420-5.

Zhang J, Qin L, Allen T & Patterson R P 2013 *The open biomedical engineering journal* **7**, 109.